



Article

# Catalyst-Assisted Large-Area Growth of Single-Crystal $\beta$ -Ga<sub>2</sub>O<sub>3</sub> Nanowires on Sapphire Substrates by Metal–Organic Chemical Vapor Deposition

Chunyang Jia <sup>1,2</sup>, Dae-Woo Jeon <sup>3</sup>, Jianlong Xu <sup>4</sup>, Xiaoyan Yi <sup>1,2</sup>, Ji-Hyeon Park <sup>3,\*</sup>  and Yiyun Zhang <sup>1,2,\*</sup> 

<sup>1</sup> R&D Center for Solid-state Lighting, Institute of Semiconductors, Chinese Academy of Sciences, Beijing 100083, China; jiachunyang16@mails.ucas.edu.cn (C.J.); spring@semi.ac.cn (X.Y.)

<sup>2</sup> Center of Materials Science and Optoelectronics Engineering, University of Chinese Academy of Sciences, Beijing 100049, China

<sup>3</sup> Korea Institute of Ceramic Engineering and Technology, 15-5, Chungmugong-dong, Jinju-si, Gyeongsongnam-do 52851, Korea; dwjeon@kicet.re.kr

<sup>4</sup> Jiangsu Key Laboratory for Carbon-Based Functional Materials & Devices, Institute of Functional Nano & Soft Materials (FUNSOM), Soochow University, Suzhou 215123, China; xujianlong@suda.edu.cn

\* Correspondence: jhp5511@kicet.re.kr (J.-H.P.); yyzhang@semi.ac.cn (Y.Z.)

Received: 28 April 2020; Accepted: 26 May 2020; Published: 28 May 2020



**Abstract:** In this work, we have achieved synthesizing large-area high-density  $\beta$ -Ga<sub>2</sub>O<sub>3</sub> nanowires on c-plane sapphire substrate by metal–organic chemical vapor deposition assisted with Au nanocrystal seeds as catalysts. These nanowires exhibit one-dimensional structures with Au nanoparticles on the top of the nanowires with lengths exceeding 6  $\mu$ m and diameters ranging from ~50 to ~200 nm. The  $\beta$ -Ga<sub>2</sub>O<sub>3</sub> nanowires consist of a single-crystal monoclinic structure, which exhibits strong  $(\bar{2}01)$  orientation, confirmed by transmission electronic microscopy and X-ray diffraction analysis. The PL spectrum obtained from these  $\beta$ -Ga<sub>2</sub>O<sub>3</sub> nanowires exhibits strong emissions centered at ~360 and ~410 nm, respectively. The energy band gap of the  $\beta$ -Ga<sub>2</sub>O<sub>3</sub> nanowires is estimated to be ~4.7 eV based on an optical transmission test. A possible mechanism for the growth of  $\beta$ -Ga<sub>2</sub>O<sub>3</sub> nanowires is also presented.

**Keywords:**  $\beta$ -Ga<sub>2</sub>O<sub>3</sub>; nanowires; MOCVD

## 1. Introduction

$\beta$ -gallium oxide ( $\beta$ -Ga<sub>2</sub>O<sub>3</sub>) is emerging as an important ultrawide bandgap semiconductor for widespread applications such as gas sensors [1,2], power electronics [3,4] and solar-blind photodetectors, due to its wider energy band gap ( $E_{gv} = \sim 4.8$  eV) and higher breakdown field strength ( $\sim 8$  MV/cm) [5–7] when compared to its counterparts SiC and GaN. As great effort has been made to achieve high-quality thin-film  $\beta$ -Ga<sub>2</sub>O<sub>3</sub> on homo/hetero substrates, the controllable growth of one-dimensional  $\beta$ -Ga<sub>2</sub>O<sub>3</sub> nanowires is promising and urgent, as it would open up new possibilities and opportunities in the scaling down of devices to achieve ultracompact nanoscale electronic devices. Moreover, compared to other phases of Ga<sub>2</sub>O<sub>3</sub>, such as  $\alpha$ -,  $\gamma$ -,  $\delta$ - and  $\kappa$ -phase,  $\beta$ -Ga<sub>2</sub>O<sub>3</sub> is the most stable and robust structure. This feature suggests  $\beta$ -Ga<sub>2</sub>O<sub>3</sub>-based nanoscale devices can function stably when used in extreme environments [8]. To address this, a variety of techniques have been employed previously to synthesize  $\beta$ -Ga<sub>2</sub>O<sub>3</sub> nanowires, including physical evaporation [9–12], arc-discharge [13], vapor–liquid–solid method (VLS) [14–16], microwave plasma [17], chemical vapor deposition (CVD) [18–20], metalorganic

chemical vapor deposition (MOCVD) [21–23], and thermal reduction method [24,25], which in all exhibit various limitations in the terms of either growth speed, large-area epitaxy or material quality. More importantly, in practice, processing of nanowire devices usually calls for precisely controlled growth of a highly-oriented nanowire array with a good uniformity in the size of individual nanowires. In the present work, a new concept of growing large-area single-crystal  $\beta$ -Ga<sub>2</sub>O<sub>3</sub> nanowires on sapphire substrate was demonstrated by using predeposited Au nano seeds as catalysts via MOCVD, which may potentially shed some light on solving this problem. We also studied the growth process of  $\beta$ -Ga<sub>2</sub>O<sub>3</sub> nanowires by performing multiple characterizations to observe the morphology, crystal structure, crystalline quality, and the growth direction of  $\beta$ -Ga<sub>2</sub>O<sub>3</sub> nanowires by scanning electron microscopy (SEM), transmission electron microscopy (TEM), selected area electron diffraction (SAED), X-ray diffraction (XRD), Raman spectroscopy, and photoluminescence (PL) spectroscopy.

## 2. Materials and Methods

### 2.1. Growth of $\beta$ -Ga<sub>2</sub>O<sub>3</sub> Nanowires

Before the Au evaporation, the sapphire substrate was cleaned in an ultrasonic bath to remove the contaminations for 5 min with organic solvents including acetone and methanol, respectively. Then, the substrate was dried using N<sub>2</sub> gun and loaded to the MOCVD reactor. A commercial horizontal-flow MOCVD system was used to grow  $\beta$ -Ga<sub>2</sub>O<sub>3</sub> nanowires on *c*-plane sapphire substrates. A conventional trimethylgallium (TMGa) bubbler and high-purity deionized (DI) vapor were used as the gallium and oxygen precursors, respectively. H<sub>2</sub> was used as the carrier gas. To start the growth, 10 nm thick Au thin film was first deposited on the sapphire substrate by e-beam evaporation. Then the wafer was loaded in the MOCVD reactor. TMGa was flowed for 1 min to predeposit gallium on the substrate before introducing the water vapor.  $\beta$ -Ga<sub>2</sub>O<sub>3</sub> nanowires were synthesized at a temperature of 690 °C with VI/III flow ratio of 300. The schematic diagram depicting catalyst-assisted large-area growth of single-crystal  $\beta$ -Ga<sub>2</sub>O<sub>3</sub> nanowires on sapphire substrate by MOCVD is illustrated in Figure 1.

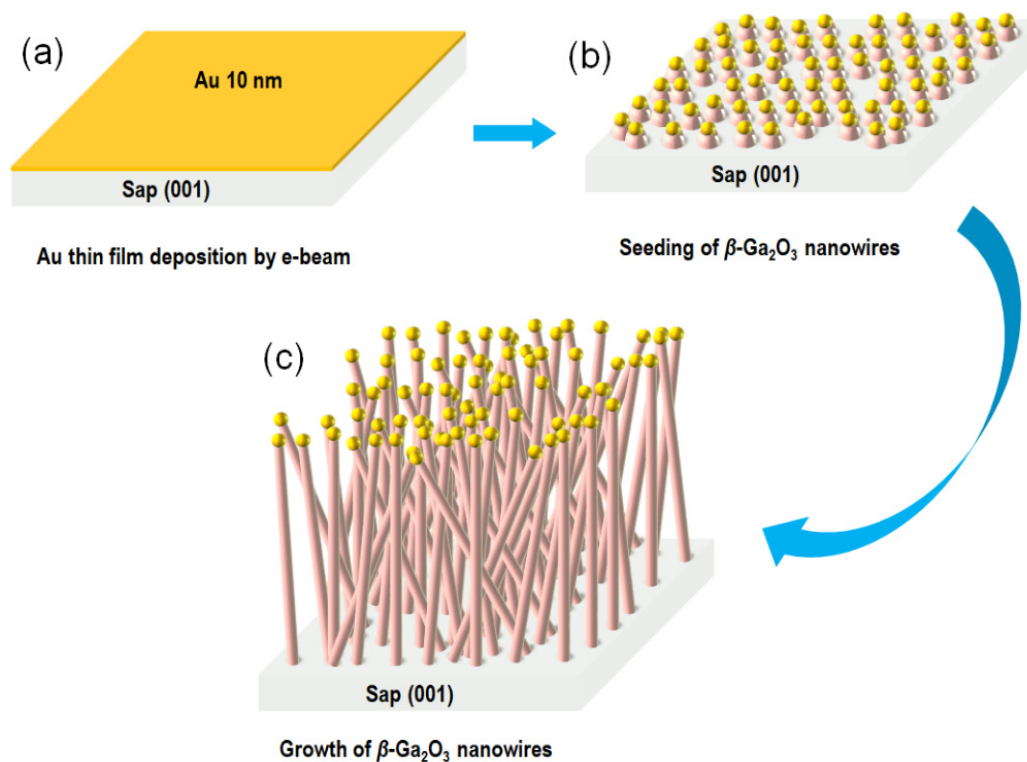


**Figure 1.** Schematic diagram depicting growth process of single-crystal  $\beta$ -Ga<sub>2</sub>O<sub>3</sub> nanowires on *c*-plane sapphire substrates by metalorganic chemical vapor deposition (MOCVD). (a) Au thin-film deposition. (b) Seeding of  $\beta$ -Ga<sub>2</sub>O<sub>3</sub> nanowires. (c) Growth of  $\beta$ -Ga<sub>2</sub>O<sub>3</sub> nanowires.

Before the root of  $\beta$ -Ga<sub>2</sub>O<sub>3</sub> nanowires was grown, due to the surface tension effect, predeposited Au thin film self-assembled into nano islands that were randomly distributed all over the sapphire substrate as the reactor chamber temperature got higher, which could be used as catalysts in the growth of  $\beta$ -Ga<sub>2</sub>O<sub>3</sub> nanowires on sapphire, with Au remaining in liquid form at this stage. [14,26] This could be apparently confirmed by the SEM images showing the growth process of  $\beta$ -Ga<sub>2</sub>O<sub>3</sub> nanowires after 5 min and 30 min, as shown in Figure 2. The inset of Figure 2a clearly illustrates a  $\beta$ -Ga<sub>2</sub>O<sub>3</sub> nanorod underneath an Au nanocrystal after 5 min growth. This growth process lasts as the nanowires get longer, while their diameters are highly consistent with the sizes of the Au nanocrystals, by which the growth direction selectivity and aspect ratio are greatly improved.

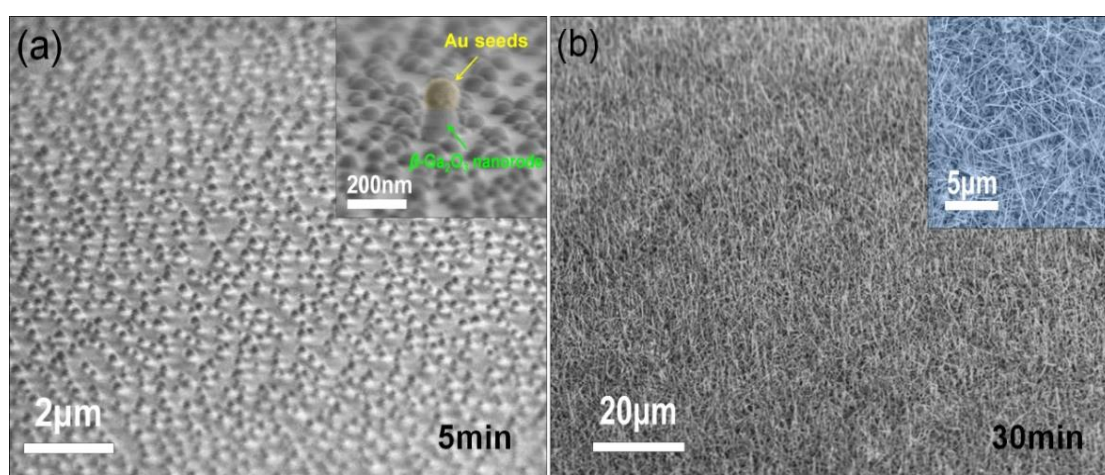


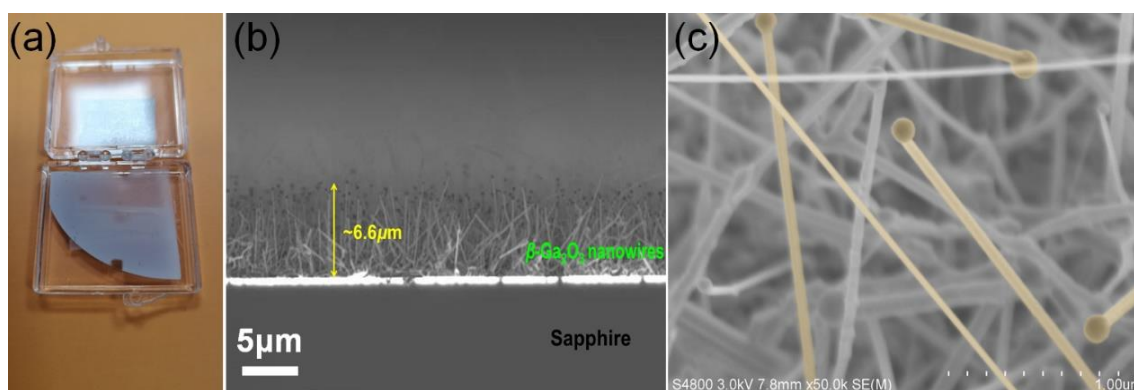
**Figure 2.** Scanning electron microscopy (SEM) images illustrating the growth process of  $\beta$ -Ga<sub>2</sub>O<sub>3</sub> nanowires (a) self-assembled Au nanocrystals as catalysts while sitting on  $\beta$ -Ga<sub>2</sub>O<sub>3</sub> nanorods after 5 min growth; inset shows a close-up SEM image of a  $\beta$ -Ga<sub>2</sub>O<sub>3</sub> nanorod under an Au nanocrystal after 5 min growth. (b) 45 degree tilted-view SEM image of  $\beta$ -Ga<sub>2</sub>O<sub>3</sub> monoclinic nanowires after 30 min growth; inset is the bird-view SEM image of  $\beta$ -Ga<sub>2</sub>O<sub>3</sub> nanowires after 30 min growth.

## 2.2. Characterization Methods

The growth process was monitored by taking the samples out of the MOCVD reactor to check the evolution of  $\beta$ -Ga<sub>2</sub>O<sub>3</sub> nanowires with SEM. As the growth finished, the orientation of  $\beta$ -Ga<sub>2</sub>O<sub>3</sub> nanowires were investigated by SEM (Hitachi S-4800), TEM (FEI Tecnai-G2-F20), Raman spectroscopy (HORIBA Scientific) and X-ray diffraction (Bede X-ray Metrology, 40 kV,  $\lambda$ :  $\sim$ 1.54 Å). A 532 nm green laser was used as the excitation source for the Raman test through an optical setup with an objective of 50 $\times$ . In each scan, the integration time was set to be 5 min for collecting Raman signals from  $\beta$ -Ga<sub>2</sub>O<sub>3</sub> nanowires. The energy band gap of  $\beta$ -Ga<sub>2</sub>O<sub>3</sub> nanowires was estimated after a numerical fitting based on the transmittance spectrum using wideband light sources (200~800 nm) as the incidence. The transitions of excited carriers were analyzed to investigate the defects and their impact on the emission characteristics for  $\beta$ -Ga<sub>2</sub>O<sub>3</sub> nanowires based on room temperature PL spectra. A 248 nm excimer laser was used as an optical pumping source and PL signals were collected by a prefocus lens and coupled into the entrance slit of a 500 mm spectrograph, dispersed by a 1200 L/mm grating to a cooled charged-coupled device (CCD), offering an optical resolution about 0.1 nm. As a comparison, a native  $\beta$ -Ga<sub>2</sub>O<sub>3</sub> substrate was also included in the PL test.

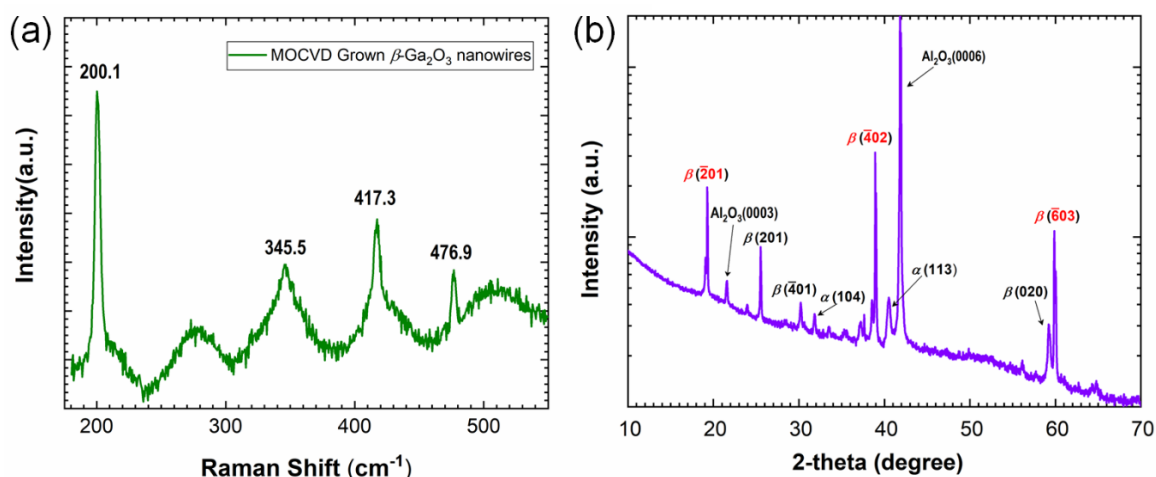
### 3. Results and Discussion

An optical image in Figure 3a presents a quarter of a 2-inch sapphire wafer with  $\beta$ -Ga<sub>2</sub>O<sub>3</sub> nanowires synthesized by MOCVD. Gray color of the wafer indicates that the nanowires are uniformly distributed on the sapphire substrate over a large area. These nanowires exhibit a nominal height of  $\sim 6.6 \mu\text{m}$ , as shown in the cross-sectional SEM image of  $\beta$ -Ga<sub>2</sub>O<sub>3</sub> nanowires on sapphire in Figure 3b. A higher magnification SEM image in Figure 3c reveals the fairly vertically-oriented growth direction of  $\beta$ -Ga<sub>2</sub>O<sub>3</sub> nanowires, with diameters ranging from  $\sim 50 \text{ nm}$  to  $\sim 200 \text{ nm}$ , indicating that the straight and long nanowires exhibit a very large aspect ratio. This is particularly true at the beginning of growth, as shown in the Figure 2b. In fact, the diameters of  $\beta$ -Ga<sub>2</sub>O<sub>3</sub> nanowires are highly depended on the sizes of Au seeds before the growth, which suggests the feasibility to tune the size and density for as-grown  $\beta$ -Ga<sub>2</sub>O<sub>3</sub> nanowires by depositing a thinner Au film for smaller and sparser Au nanoseeds. In addition, we can clearly observe that the spherical-shaped Au nanoparticles are sitting on the stem of the nanowire at the tips, which again confirms the growth mechanism as described before. The growth rate of nanowire in the vertical direction can be roughly estimated as 200 nm/min.



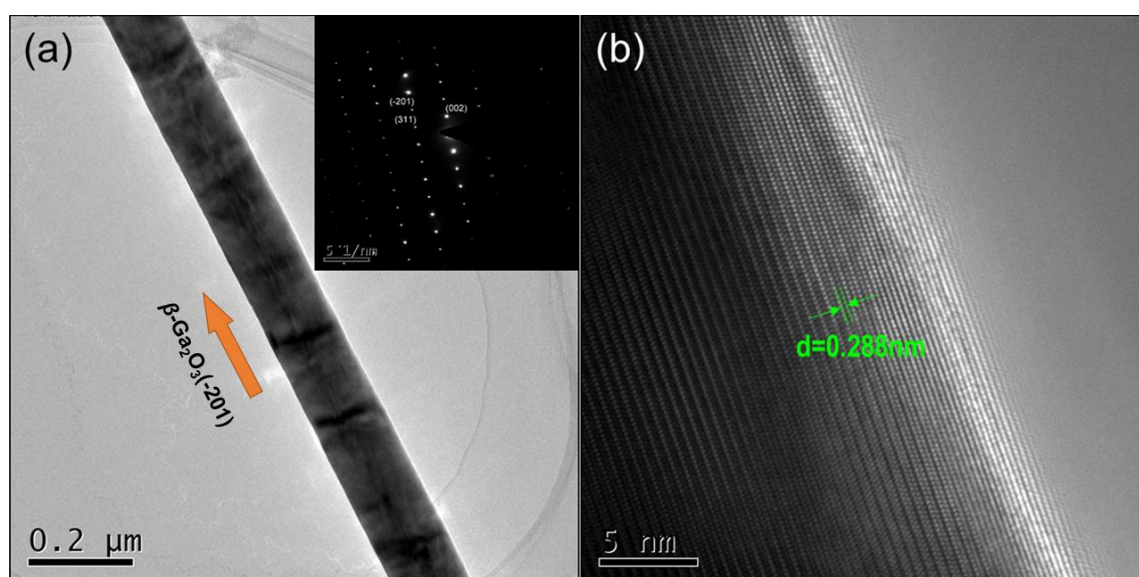
**Figure 3.** (a) A quarter of 2-inch as-grown  $\beta$ -Ga<sub>2</sub>O<sub>3</sub> nanowires on sapphire wafer. (b) Cross-sectional SEM image of the as-grown  $\beta$ -Ga<sub>2</sub>O<sub>3</sub> nanowires. (c) High-magnification SEM image of nanowires.

Raman analysis was performed to analyze the crystal structure on typical  $\beta$ -Ga<sub>2</sub>O<sub>3</sub> nanowire samples. It can be seen that strong and sharp Raman peaks from crystalline Ga\O bonds are centered at 200.1, 345.5, 476.9 and 417.3  $\text{cm}^{-1}$  in Figure 4a. This spectrum demonstrates that the nanowires present the monoclinic  $\beta$ -Ga<sub>2</sub>O<sub>3</sub> phase and have a very good crystal quality [27,28]. Meanwhile, XRD was used to examine the crystal structure of the large-area  $\beta$ -Ga<sub>2</sub>O<sub>3</sub> nanowires grown by MOCVD. A typical XRD pattern of as-grown sample is shown in Figure 4b. The peaks at 21° and 41° correspond to the {0001} diffraction peaks of the sapphire substrate. In addition, three dominant diffraction peaks at 18.9°, 38.4° and 59.2° are observed, which correspond to the ( $\bar{2}$ 01), ( $\bar{4}$ 02), and ( $\bar{6}$ 03) planes of  $\beta$ -Ga<sub>2</sub>O<sub>3</sub>, respectively. It illustrates that the  $\beta$ -Ga<sub>2</sub>O<sub>3</sub> nanowires are mostly ( $\bar{2}$ 01)-oriented, which is almost paralleled to the sapphire (0001) plane [29]. Three much weaker peaks correspond to the (201), ( $\bar{4}$ 01), and (020) planes of  $\beta$ -Ga<sub>2</sub>O<sub>3</sub>. It again affirms that the as-grown vertically-oriented  $\beta$ -Ga<sub>2</sub>O<sub>3</sub> nanowires have the monoclinic structure ( $\beta$ -Ga<sub>2</sub>O<sub>3</sub> ( $a = 12.12\text{--}12.34$ ,  $b = 3.03\text{--}3.04$ ,  $c = 5.78\text{--}5.87$ )), according to the Joint Committee on Powder Diffraction Standards (JCPDS) powder diffraction file No. 76-0573. [29,30]. The growth temperature (690 °C) may contribute to the diffraction peaks of the  $\alpha$ -phase Ga<sub>2</sub>O<sub>3</sub> nanowires in Figure 4b [31].



**Figure 4.** (a) Raman and (b) X-ray diffraction (XRD) spectra of  $\beta$ - $\text{Ga}_2\text{O}_3$  nanowires.

In order to further investigate the detailed crystal structure of the as-grown sample, Figure 5a presents a typical TEM image of an individual synthesized  $\beta$ - $\text{Ga}_2\text{O}_3$  nanowire with a diameter of about 80 nm. The selected area electron diffraction (SAED) shown in the inset of Figure 5a confirms that the synthesized sample shows perfect crystallinity of monoclinic  $\beta$ - $\text{Ga}_2\text{O}_3$ . Figure 5b presents a high resolution TEM (HRTEM) image of the  $\beta$ - $\text{Ga}_2\text{O}_3$  nanowires. The lattice fringes with a  $d$  spacing of 0.288 nm are observed, which corresponds to the (004) lattice planes of  $\beta$ - $\text{Ga}_2\text{O}_3$ . The  $\beta$ - $\text{Ga}_2\text{O}_3$  nanowires of the same direction as the white arrow grow along the  $(\bar{2}01)$  direction, which is consistent with the results given in Figure 5a.



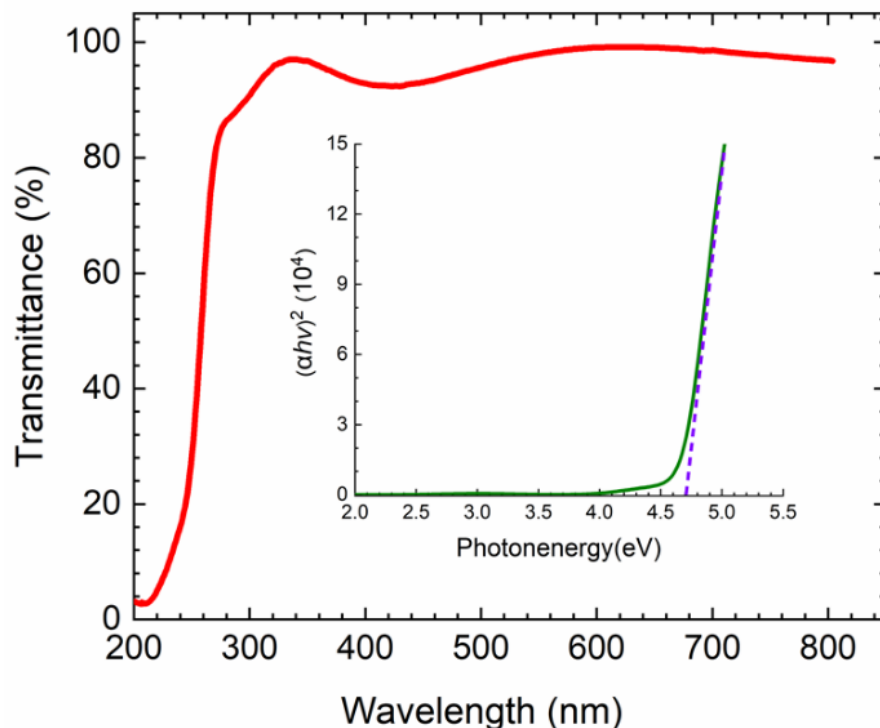
**Figure 5.** (a) Transmission electron microscopy (TEM) image of an individual  $\beta$ - $\text{Ga}_2\text{O}_3$  nanowire. The typical electron diffraction pattern is in the inset. (b) High-resolution TEM image of the  $\beta$ - $\text{Ga}_2\text{O}_3$  nanowires with uniform lattice fringes.

Figure 6 presents the optical transmittance of the  $\beta$ - $\text{Ga}_2\text{O}_3$  nanowires. It can be clearly observed that the band-edge absorption for the as-grown  $\beta$ - $\text{Ga}_2\text{O}_3$  nanowires is at about 275 nm, from which the band gap can be roughly estimated as 4.53 eV by using the equation:  $E_g = 1240/\lambda$ . Moreover, it has a much lower absorption in the visible region when compared with the sharp band-edge absorption in the deep ultraviolet region below 280 nm, suggesting great potential for being used as solar-blind photodetectors for these nanowires. For a more accurate estimate, the optical band gap of the  $\beta$ - $\text{Ga}_2\text{O}_3$

nanowires is calculated by extrapolating the linear portion of the square of absorption coefficient against photon energy using the equation:

$$(\alpha h\nu)^2 = B \cdot (h\nu - E_g) \quad (1)$$

where  $\alpha$  is absorption coefficient,  $h$  is the Planck's constant, and  $\nu$  is the frequency of the incident light, and  $B$  is a constant [7,32–34]. The band gap of  $\beta$ -Ga<sub>2</sub>O<sub>3</sub> nanowires is estimated to be  $\sim 4.7$  eV as shown in the inset of Figure 6. This value is in agreement with the band gaps from experiments ranging from 4.6 to 4.9 eV as reported by others [29]. It is also consistent with theoretical predictions of a direct band gap at  $\Gamma$ -point ( $E_g(\Gamma-\Gamma)$ ,  $\sim 4.8 \pm 0.1$  eV) and indirect band gap at L-point ( $E_g(\Gamma-L)$ ,  $\sim 4.7 \pm 0.1$  eV) by quasiparticle self-consistent GW calculations for  $\beta$ -Ga<sub>2</sub>O<sub>3</sub> [35].



**Figure 6.** Optical transmission spectrum of the  $\beta$ -Ga<sub>2</sub>O<sub>3</sub> nanowires.  $(\alpha h\nu)^2$  versus photon energy plots of the  $\beta$ -Ga<sub>2</sub>O<sub>3</sub> nanowires in the inset.

Figure 7 shows the PL spectrum obtained from  $\beta$ -Ga<sub>2</sub>O<sub>3</sub> nanowires and native  $\beta$ -Ga<sub>2</sub>O<sub>3</sub> (-201) substrate at room temperature at the same pumping conditions. For removing the artifacts from the laser sources, the PL spectrum from the nanowires is baseline-fitted. In the baseline fitting, to identify the intrinsic emission, the PL spectrum of nanowires is separated from the laser excitation background, as the intrinsic emissions of  $\beta$ -Ga<sub>2</sub>O<sub>3</sub> is greatly overlapped with laser excitation background (see Figure 7). Emission spectral peaks centered at  $\sim 257$  nm and  $\sim 275$  nm can be observed, which correspond with the band-edge transitions of excited carriers that originate from the anisotropy of the monoclinic phase [36]. Aside from the band-edge emission,  $\beta$ -Ga<sub>2</sub>O<sub>3</sub> nanowires exhibit two distinct spectral peaks at  $\sim 360$  nm and  $\sim 410$  nm, respectively, which are consistent with the PL spectral peaks of native  $\beta$ -Ga<sub>2</sub>O<sub>3</sub> (-201) substrate. The peak at 360 nm is originated from recombination processes caused by self-trapped holes (STH), which is an intrinsic feature and is not due to defects. The spectral peak located at 410 nm is related to the recombination of donor–acceptor pairs (DAP), which is a result of electrons tunneling from the donor to the acceptor when photo-generated carriers are captured by donors or acceptors in  $\beta$ -Ga<sub>2</sub>O<sub>3</sub>. A weak spectral peak can be identified at  $\sim 440$  nm for the  $\beta$ -Ga<sub>2</sub>O<sub>3</sub> nanowires, corresponding to the blue band emission that strongly correlates with oxygen vacancy

concentration [37]. Overall, the PL spectrum from  $\beta$ -Ga<sub>2</sub>O<sub>3</sub> nanowires is highly consistent with that from native  $\beta$ -Ga<sub>2</sub>O<sub>3</sub> substrate, which suggests high material quality of as-grown  $\beta$ -Ga<sub>2</sub>O<sub>3</sub> nanowires.

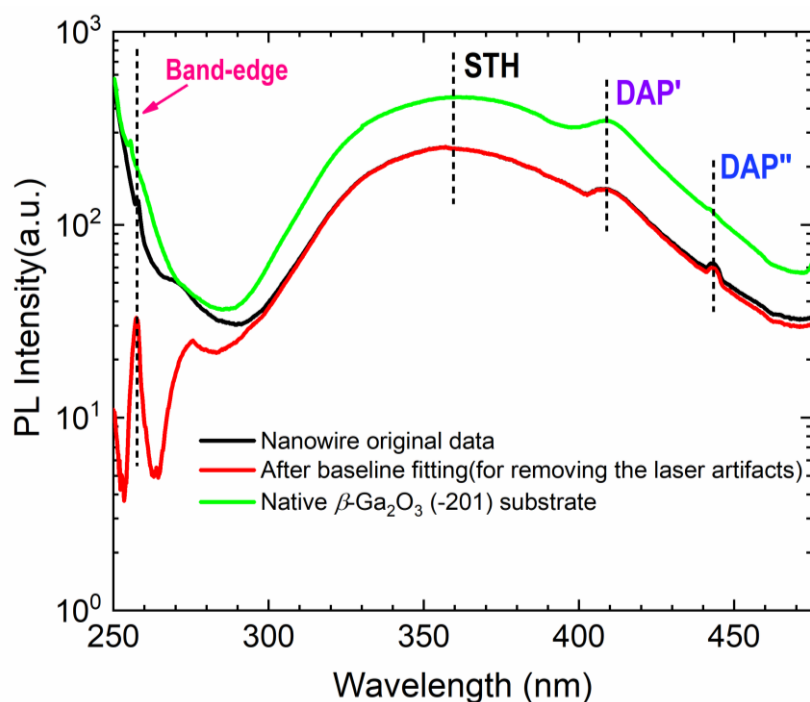


**Figure 7.** Room temperature photoluminescence (PL) spectra of  $\beta$ -Ga<sub>2</sub>O<sub>3</sub> nanowires and native  $\beta$ -Ga<sub>2</sub>O<sub>3</sub> substrate at the same optical excitation conditions.

#### 4. Conclusions

In summary, we have presented a new method to grow large-area single-crystal monoclinic  $\beta$ -Ga<sub>2</sub>O<sub>3</sub> nanowires by MOCVD. Assisted by Au nanocrystal seeds as catalysts, the growth of nanowires exhibited a very good selectivity in the  $(\bar{2}01)$  direction, which demonstrates an array of  $>6 \mu\text{m}$  long one-dimensional nanowires. Diameters of the nanowires are highly depended on the sizes of Au nano particles, ranging from  $\sim 50$  to  $\sim 200$  nm. The room temperature PL spectrum obtained from  $\beta$ -Ga<sub>2</sub>O<sub>3</sub> nanowires exhibits strong emissions centered at  $\sim 360$  and  $\sim 410$  nm, representing the recombination processes via electrons/self-trapped holes and donor–acceptor pairs, respectively, while the blue band emission was greatly suppressed with less O vacancies in  $\beta$ -Ga<sub>2</sub>O<sub>3</sub> nanowires. The energy band gap of the  $\beta$ -Ga<sub>2</sub>O<sub>3</sub> nanowires is estimated to be 4.7 eV according to the optical transmission test. Our method suggests a great potential in realizing controllable growth of  $\beta$ -Ga<sub>2</sub>O<sub>3</sub> nanowires by predepositing highly-ordered Au nanoplates for arrayed growth. This work provides a new thought on the synthesis of high-quality  $\beta$ -Ga<sub>2</sub>O<sub>3</sub> nanowires that facilitates the scaling down in the perspective of fabricating  $\beta$ -Ga<sub>2</sub>O<sub>3</sub>-based field-effect transistors and solar-blind photodetectors.

**Author Contributions:** Conceptualization, J.-H.P. and Y.Z.; formal analysis, C.J., J.-H.P. and Y.Z.; funding acquisition, Y.Z.; investigation, C.J., J.X., J.-H.P. and Y.Z.; methodology, J.-H.P. and Y.Z.; project administration, D.-W.J.; supervision, X.Y., J.-H.P. and Y.Z.; writing—original draft, C.J. and Y.Z.; writing—review and editing, J.-H.P. and Y.Z. All authors have read and agreed to the published version of the manuscript.

**Funding:** This research was funded by Chinese Academy of Sciences.

**Acknowledgments:** This research was supported by Basic Science Research Program through the National Research Foundation of Korea (NRF) funded by the Ministry of Education (No. 2018R1D1A1B07048429).

**Conflicts of Interest:** The authors declare no conflict of interest.

## References

1. Mazeina, L.; Picard, Y.N.; Maximenko, S.I.; Perkins, F.K.; Glaser, E.R.; Twigg, M.E.; Freitas, J.A.; Prokes, S.M. Growth of Sn-Doped  $\beta$ -Ga<sub>2</sub>O<sub>3</sub> Nanowires and Ga<sub>2</sub>O<sub>3</sub>-SnO<sub>2</sub> Heterostructures for Gas Sensing Applications. *Cryst. Growth Des.* **2009**, *9*, 4471–4479. [[CrossRef](#)]
2. Kim, H.; Jin, C.; An, S.; Lee, C. Fabrication and CO Gas-sensing Properties of Pt-functionalized Ga<sub>2</sub>O<sub>3</sub> Nanowires. *Ceram. Int.* **2012**, *38*, 3563–3567. [[CrossRef](#)]
3. Higashiwaki, M.; Sasaki, K.; Kuramata, A.; Masui, T.; Yamakoshi, S. Development of Gallium Oxide Power Devices. *Phys. Status Solidi A* **2014**, *211*, 21–26. [[CrossRef](#)]
4. Higashiwaki, M.; Kuramata, A.; Murakami, H.; Kumagai, Y. State-of-the-art Technologies of Gallium Oxide Power Devices. *J. Phys. D: Appl. Phys.* **2017**, *50*, 333002. [[CrossRef](#)]
5. Feng, P.; Zhang, J.Y.; Li, Q.H.; Wang, T.H. Individual  $\beta$ -Ga<sub>2</sub>O<sub>3</sub> nanowires as solar-blind photodetectors. *Appl. Phys. Lett.* **2006**, *88*, 153107. [[CrossRef](#)]
6. Wang, S.; Sun, H.; Wang, Z.; Zeng, X.; Ungar, G.; Guo, D.; Shen, J.; Li, P.; Liu, A.; Li, C.; et al. In Situ Synthesis of Monoclinic  $\beta$ -Ga<sub>2</sub>O<sub>3</sub> Nanowires on Flexible Substrate and Solar-blind Photodetector. *J. Alloys Compd.* **2019**, *787*, 133–139. [[CrossRef](#)]
7. Chen, Y.-C.; Lu, Y.-J.; Liu, Q.; Lin, C.-N.; Guo, J.; Zang, J.-H.; Tian, Y.-Z.; Shan, C.-X. Ga<sub>2</sub>O<sub>3</sub> Photodetector Arrays for Solar-blind Imaging. *J. Mater. Chem. C* **2019**, *7*, 2557–2562. [[CrossRef](#)]
8. Wei, T.-C.; Tsai, D.-S.; Ravadgar, P.; Ke, J.-J.; Tsai, M.-L.; Lien, D.-H.; Huang, C.-Y.; Horng, R.-H.; He, J.-H. See-Through Ga<sub>2</sub>O<sub>3</sub> Solar-Blind Photodetectors for Use in Harsh Environments. *IEEE J. Select. Top. Quantum Electron.* **2014**, *20*, 112–117. [[CrossRef](#)]
9. Zhang, H.Z.; Kong, Y.C.; Wang, Y.Z.; Du, X.; Bai, Z.G.; Wang, J.J.; Yu, D.P.; Ding, Y.; Hang, Q.L.; Feng, S.Q. Ga<sub>2</sub>O<sub>3</sub> Nanowires Prepared by Physical Evaporation. *Solid State Commun.* **1999**, *109*, 677–682. [[CrossRef](#)]
10. Nogales, E.; García, J.Á.; Méndez, B.; Piqueras, J. Doped Gallium Oxide Nanowires with Waveguiding Behavior. *Appl. Phys. Lett.* **2007**, *91*, 133108. [[CrossRef](#)]
11. Gonzalo, A.; Nogales, E.; Méndez, B.; Piqueras, J. Influence of Growth Temperature on the Morphology and Luminescence of Ga<sub>2</sub>O<sub>3</sub>:Mn Nanowires. *Phys. Status Solidi A* **2014**, *211*, 494–497. [[CrossRef](#)]
12. Gonzalo, A.; Nogales, E.; Lorenz, K.; Villora, E.G.; Shimamura, K.; Piqueras, J.; Méndez, B. Raman and Cathodoluminescence Analysis of Transition Metal Ion Implanted Ga<sub>2</sub>O<sub>3</sub> Nanowires. *J. Lumin.* **2017**, *191*, 56–60. [[CrossRef](#)]
13. Park, G.-S.; Choi, W.-B.; Kim, J.-M.; Choi, Y.C.; Lee, Y.H.; Lim, C.-B. Structural Investigation of Gallium Oxide ( $\beta$ -Ga<sub>2</sub>O<sub>3</sub>) Nanowires Grown by Arc-discharge. *J. Cryst. Growth* **2000**, *220*, 494–500. [[CrossRef](#)]
14. Cha, S.Y.; Ahn, B.-G.; Kang, H.C.; Lee, S.Y.; Noh, D.Y. Direct Conversion of  $\beta$ -Ga<sub>2</sub>O<sub>3</sub> Thin Films to  $\beta$ -Ga<sub>2</sub>O<sub>3</sub> Nanowires by Annealing in a Hydrogen Atmosphere. *Ceram. Int.* **2018**, *44*, 16470–16474. [[CrossRef](#)]
15. Chang, K.-W.; Wu, J.-J. Low-Temperature Growth of Well-Aligned  $\beta$ -Ga<sub>2</sub>O<sub>3</sub> Nanowires from a Single-Source Organometallic Precursor. *Adv. Mater.* **2004**, *16*, 545–549. [[CrossRef](#)]
16. Liang, C.H.; Meng, G.W.; Wang, G.Z.; Wang, Y.W.; Zhang, L.D.; Zhang, S.Y. Catalytic Synthesis and Photoluminescence of  $\beta$ -Ga<sub>2</sub>O<sub>3</sub> Nanowires. *Appl. Phys. Lett.* **2001**, *78*, 3202–3204. [[CrossRef](#)]
17. Sharma, S.; Sunkara, M.K. Direct Synthesis of Gallium Oxide Tubes, Nanowires, and Nanopaintbrushes. *J. Am. Chem. Soc.* **2002**, *124*, 12288–12293. [[CrossRef](#)]
18. Chun, H.J.; Choi, Y.S.; Bae, S.Y.; Seo, H.W.; Hong, S.J.; Park, J.; Yang, H. Controlled Structure of Gallium Oxide Nanowires. *J. Phys. Chem. B* **2003**, *107*, 9042–9046. [[CrossRef](#)]
19. Kumar, M.; Kumar, V.; Singh, R. Diameter Tuning of  $\beta$ -Ga<sub>2</sub>O<sub>3</sub> Nanowires Using Chemical Vapor Deposition Technique. *Nanoscale Res. Lett.* **2017**, *12*, 184. [[CrossRef](#)]
20. Ning, J.Q.; Xu, S.J.; Wang, P.W.; Song, Y.P.; Yu, D.P.; Shan, Y.Y.; Lee, S.T.; Yang, H. Microstructure and Micro-Raman Studies of Nitridation and Structure transition of Gallium Oxide Nanowires. *Mater. Charact.* **2012**, *73*, 153–157. [[CrossRef](#)]
21. Kim, H.W.; Kim, N.H. Formation of Amorphous and Crystalline Gallium Oxide Nanowires by Metalorganic Chemical Vapor Deposition. *Appl. Surf. Sci.* **2004**, *233*, 294–298. [[CrossRef](#)]
22. Kim, H.W.; Shim, S.H. Characteristics of Gallium Oxide Nanowires Synthesized by the Metalorganic Chemical Vapor Deposition. *MSF* **2007**, *539–543*, 1230–1235. [[CrossRef](#)]
23. Kim, N.H.; Kim, H.W.; Seoul, C.; Lee, C. Amorphous Gallium Oxide Nanowires Synthesized by Metalorganic Chemical Vapor Deposition. *Mater. Sci. Eng. B* **2004**, *111*, 131–134. [[CrossRef](#)]

24. Wu, X.C.; Song, W.H.; Huang, W.D.; Pu, M.H.; Zhao, B.; Sun, Y.P.; Du, J.J. Crystalline Gallium Oxide Nanowires: Intensive Blue Light Emitters. *Chem. Phys. Lett.* **2000**, *328*, 5–9. [[CrossRef](#)]
25. Quan, Y.; Fang, D.; Zhang, X.; Liu, S.; Huang, K. Synthesis and Characterization of Gallium Oxide Nanowires via a Hydrothermal Method. *Mater. Chem. Phys.* **2010**, *121*, 142–146. [[CrossRef](#)]
26. Sadan, H.; Kaplan, W.D. Au–Sapphire (0001) Solid–solid Interfacial Energy. *J. Mater. Sci.* **2006**, *41*, 5099–5107. [[CrossRef](#)]
27. Rao, R.; Rao, A.M.; Xu, B.; Dong, J.; Sharma, S.; Sunkara, M.K. Blue Shifted Raman Scattering and Its Correlation with the [110] Growth Direction in Gallium Oxide Nanowires. *J. Appl. Phys.* **2005**, *98*, 94312. [[CrossRef](#)]
28. Dohy, D.; Lucazeau, G.; Revcolevschi, A. Raman Spectra and Valence Force Field of Single-crystalline  $\beta$ -Ga<sub>2</sub>O<sub>3</sub>. *J. Solid State Chem.* **1982**, *45*, 180–192. [[CrossRef](#)]
29. Nakagomi, S.; Kokubun, Y. Crystal Orientation of  $\beta$ -Ga<sub>2</sub>O<sub>3</sub> Thin Films Formed on C-plane and A-plane Sapphire Substrate. *J. Cryst. Growth* **2012**, *349*, 12–18. [[CrossRef](#)]
30. Pearton, S.J.; Yang, J.; Cary, P.H.; Ren, F.; Kim, J.; Tadjer, M.J.; Mastro, M.A. A Review of Ga<sub>2</sub>O<sub>3</sub> Materials, Processing, and Devices. *Appl. Phys. Rev.* **2018**, *5*, 11301. [[CrossRef](#)]
31. Oshima, T.; Okuno, T.; Fujita, S. Ga<sub>2</sub>O<sub>3</sub> Thin Film Growth on c-Plane Sapphire Substrates by Molecular Beam Epitaxy for Deep-Ultraviolet Photodetectors. *Jpn. J. Appl. Phys.* **2007**, *46*, 7217–7220. [[CrossRef](#)]
32. Zhang, Y.; Yan, J.; Li, Q.; Qu, C.; Zhang, L.; Xie, W. Optical and Structural Properties of Cu-doped  $\beta$ -Ga<sub>2</sub>O<sub>3</sub> Films. *Mat. Sci. Eng. B* **2011**, *176*, 846–849. [[CrossRef](#)]
33. Liu, Q.; Guo, D.; Chen, K.; Su, Y.; Wang, S.; Li, P.; Tang, W. Stabilizing the Metastable  $\gamma$  Phase in Ga<sub>2</sub>O<sub>3</sub> Thin Films by Cu Doping. *J. Alloys Compd.* **2018**, *731*, 1225–1229. [[CrossRef](#)]
34. Huang, L.; Feng, Q.; Han, G.; Li, F.; Li, X.; Fang, L.; Xing, X.; Zhang, J.; Hao, Y. Comparison Study of  $\beta$ -Ga<sub>2</sub>O<sub>3</sub> Photodetectors Grown on Sapphire at Different Oxygen Pressures. *IEEE Photonics J.* **2017**, *9*, 1–8. [[CrossRef](#)]
35. Ratnaparkhe, A.; Lambrecht, W.R.L. Quasiparticle Self-consistent GW Band Structure of  $\beta$ -Ga<sub>2</sub>O<sub>3</sub> and the Anisotropy of the Absorption Onset. *Appl. Phys. Lett.* **2017**, *110*, 132103. [[CrossRef](#)]
36. Li, Y.; Tokizono, T.; Liao, M.; Zhong, M.; Koide, Y.; Yamada, I.; Delaunay, J.-J. Efficient Assembly of Bridged  $\beta$ -Ga<sub>2</sub>O<sub>3</sub> Nanowires for Solar-Blind Photodetection. *Adv. Funct. Mater.* **2010**, *20*, 3972–3978. [[CrossRef](#)]
37. McCluskey, M.D. Point Defects in Ga<sub>2</sub>O<sub>3</sub>. *J. Appl. Phys.* **2020**, *127*, 101101. [[CrossRef](#)]



© 2020 by the authors. Licensee MDPI, Basel, Switzerland. This article is an open access article distributed under the terms and conditions of the Creative Commons Attribution (CC BY) license (<http://creativecommons.org/licenses/by/4.0/>).